NUCLEAR THEORY, Vol. 36 (2017)
eds. M. Gaidarov, N. Minkov, Heron Press, Sofia

Chiral Effective Field Theory in Nucleonic Matter

F. Sammarruca

University of Idaho, 83844-0903 Moscow, Idaho, U.S.A.

Abstract. We review predictions for the interaction part of the symmetry energy from different microscopic approaches and compare them with updated constraints recently extracted at GSI. The discussion is then extended to the neutron skin thickness in ^{208}Pb and its relation to the density derivative of the symmetry energy. We also discuss briefly some preliminary neutron star predictions we have obtained based on chiral nuclear forces.

1 Introduction

The energy per particle as a function of density in infinite nuclear matter, known as the equation of state (EoS), contains rich information about the nature of the nuclear force in hadronic medium. Selected reaction observables and other nuclear properties have been found to be sensitive to the EoS, and therefore their measurements can provide useful constraints for the latter. The well-known expression for the EoS of isospin asymmetric matter as a function of the neutron excess parameter brings into focus the *symmetry energy*, a quantity of fundamental importance for a variety of neutron-rich systems. Presently our knowledge of the symmetry energy is limited, particularly its density dependence around and above saturation density. From the experimental side, heavy-ion (HI) reactions are an established way to seek such constraints, based on the fact that the EoS is an important part of the input in transport models describing HI collisions.

Other nuclear properties have been found highly sensitive to specific aspects of the EoS of asymmetric matter. The neutron skin thickness, for instance, is sensitive to the slope of the symmetry energy, which, in turn, determines the pressure which pushes neutrons towards the outer region to form the skin. A strong correlation is also found between the pressure in the interior of a heavy nucleus and the radius of the average-mass neutron star.

Earlier data from the FOPI-LAND experiment [1, 2] were reanalysed in Ref. [3] and compared with transport model calculations. Those analyses suggested a softer-than-linear to linear term for the potential energy part of the symmetry energy, the latter being parametrized as a power law. More recently, the directed and elliptic flows of neutrons and light charged particles in the reaction ^{197}Au + ^{197}Au at 400 MeV per nucleon were measured in the ASY-EOS experiment at GSI [4]. The updated findings confirm a moderately soft density

dependence, but in Ref. [4] the authors report a more stringent constraint up to twice normal density.

As updated constraints have become available, comparison with microscopic calculations is especially important and timely. Within that spirit, modern predictions of the symmetry energy based on chiral effective field theory (EFT) [5] are reviewed and discussed, following closely Ref. [6]. For comparison, other approaches are also considered, such as those based on meson-theoretic or phenomenological nucleon-nucleon (NN) potentials and three-nucleon forces (3NF). These approaches, which were particularly popular in the 1990's and are still frequently used today, follow a very different philosophy. Thus, their inclusion in the comparison will provide a realistic measure of the spreading of contemporary theoretical predictions.

Before proceeding, we recall that the parametrization used in the analysis of Ref. [4] is

$$e_{sym}(\rho) = 22\ \mathrm{MeV}\Big(\frac{\rho}{\rho_0}\Big)^{\gamma} + 12\ \mathrm{MeV}\Big(\frac{\rho}{\rho_0}\Big)^{2/3}\ , \tag{1}$$

which fixes the symmetry energy at ρ_0 to be 34 MeV. The power law coefficient, γ, is reported as 0.72 ± 0.19. The same coefficient was found to be 0.9 ± 0.4 from the FOPI-LAND data [1–3]. Other useful quantities for the discussion which follows are the so-called "L" coefficient,

$$L = 3\rho_0\Big(\frac{\partial e_{sym}}{\partial \rho}\Big)_{\rho_0}\ , \tag{2}$$

and the obviously related symmetry pressure, $P_0 = \rho_0 L/3$.

Recalling the remarkable correlation between neutron skins and the radii of compact stars, due to the chief role that neutron matter pressure plays in both systems, we close the paper with a brief discussion of some preliminary predictions of neutron star radii based on chiral EFT [7].

2 Theoretical Input

2.1 The chiral EoS

Chiral EFT is presently a popular approach which starts from a low-energy realization of quantum chromodynamics [5]. In chiral EFT, one retains the basic degrees of freedom typical of low-energy nuclear physics, pions and nucleons, while fitting unresolved nuclear dynamics at short distances to the properties of two- and few-nucleon systems. More specifically, EFT is a theory in which the properties governed by low-energy physics are specified by the choice of degrees of freedom and symmetries, and can be computed systematically. Short-range physics is included through the processes of regularization and renormalization. The microscopic EoS of symmetric nuclear matter and neutron matter based on chiral EFT employed here are calculated as described in Ref. [8]. The predictions at next-to-next-to-next-to-leading order ($\mathrm{N^3LO}$) and at next-to-next-to-leading order ($\mathrm{N^2LO}$) are based on high-precision chiral NN potentials at

the respective orders [9] together with the leading 3NF, which is treated as in Ref. [10].

Since estimating the truncation error at N^{3}LO requires the predictions at N^{2}LO, those will be shown as well. (N^{4}LO predictions are not yet available.) Note that the N^{2}LO calculation is complete, in the sense that both the two-nucleon force (2NF) and the 3NF are consistently at next-to-next-to-leading order. This is not the case, though, for the N^{3}LO calculation, where the 3NF at N^{2}LO is employed.

2.2 Relativistic meson-theoretic potentials and the Dirac–Brueckner–Hartree–Fock approach to the equation of state

In contrast to conventional Brueckner theory, the relativistic approach to nuclear matter, particularly the Dirac-Brueckner-Hartree-Fock (DBHF) approximation, has the inherent ability to predict realistic values for the saturation energy and density of nuclear matter. The characteristic feature of the DBHF approach is the fact that important 3NF are effectively taken into account through the density dependence of the nucleon spinors. This effective 3NF, which originates from virtual excitations of nucleon-antinucleon pairs, provides a strong (repulsive and density-dependent) saturating effect and, thus, an important mechanism missing from conventional Brueckner-Hartree-Fock calculations. For a recent review, including considerations of isospin asymmetry, see Ref. [11].

2.3 Variational approaches

Alternatively, the energy per particle in nuclear matter can be obtained combining the 2NF with meson-theoretic or phenomelogical 3NF to generate the additional repulsion essential to improve saturation. Nonrelativistic calculations of symmetric and neutron matter based on variational methods [12] and phenomenological 2NF and 3NF have been used extensively. We also represent this point of view by including predictions [13] based on popular phenomenological 2NF and 3NF from the 90's, namely the Argonne v_{18} NN potential [14] together with the Urbana model IX [15] 3NF. These will be referred to as the "APR" predictions.

3 Predictions and Discussion

We calculate the symmetry energy for the theories and models mentioned in the previous section and subtract the kinetic contribution. The microscopic values of the potential energy part are then fitted with a power law. for each of the models being considered, ρ_0 is the actual saturation density for that particular EoS.

In Figure 1, we display the potential energy part of the symmetry energy as obtained from microscopic calculations at N^{2}LO (solid green line) and at N^{3}LO (solid red line), together with approximations given by functions of the form

$$e_{sym}^{pot} = V_0(\rho/\rho_0)^\gamma \ , \tag{3}$$

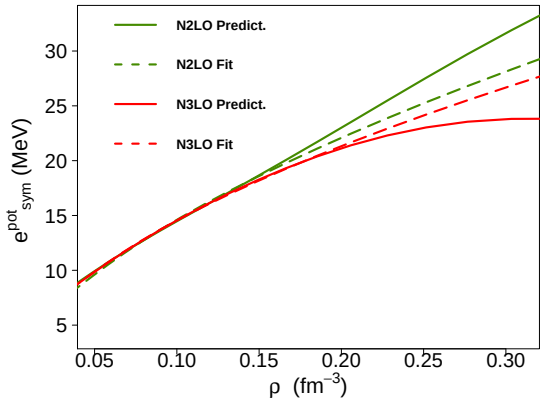

Figure 1. Microscopic predictions of the interaction part of the symmetry energy at N^{2}LO and N^{3}LO of chiral perturbation theory, and corresponding power-law fits. See inset for the definition of the various curves.

dashed green for N^{2}LO and dashed red for N^{3}LO. The fit is done by searching for the single parameter γ, setting V_0 equal to the microscopically predicted value at the appropriate saturation density. The density range considered in the fit covers approximately from 0.03 to 0.33 fm^{-3}, with all points carrying the same weight.

The theoretical predictions appear reasonably described by the simple *ansatz* up to their respective saturation densities and somewhat above it, whereas the constraint should be applicable up to about $2\rho_0$, which amounts to approximately 0.3 fm^{-3} by the definition of Ref. [4]. Similar considerations apply to the fits of the symmetry energies obtained from the other EoS (DBHF and APR), see Ref. [6].

With regard to the N^{3}LO predictions, it is important to keep in mind that they must be seen in the context of EFT theoretical uncertainties. Therefore, in Figure 2 the N^{3}LO predictions are shown with their estimated truncation error. In Figure 2, the shaded area represents the empirical constraint. The predictions fall within the empirical constraints at the lower densities but are otherwise softer.

Although the parametrization given in Eq. 1 was found to be consistent with the reaction observables measured in the GSI experiment, here we observe that it would be interesting to move beyond the power-law parametrization when analyzing elliptic-flow data. A moderately soft (less than linear) dependence is, indeed, preferred by microscopic models, but Eq. 1 is overall not a satisfactory representation of these theoretical predictions.

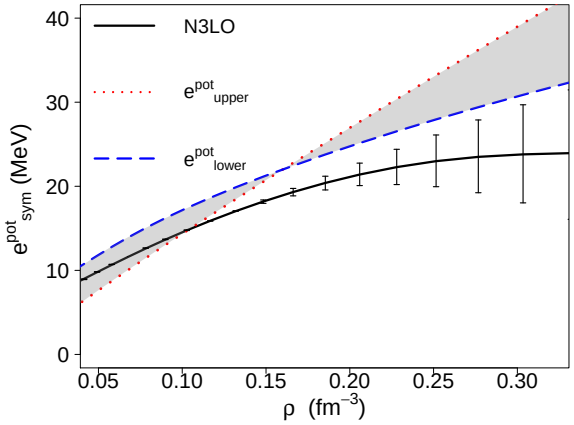

Figure 2. Microscopic predictions of the interaction part of the symmetry energy at N^{3}LO with EFT truncation error. The shaded area shows the empirical constraint from Ref. [4].

Next we extend the discussion to the neutron skin of ^{208}Pb in relation to density derivatives and pressure. The reader is referred to Ref. [6] and references therein for details on the neutron skin calculations.

In Table 1, for values of γ spanning the uncertainty of the ASY-EOS constraint, we show (second, fourth, and fifth columns, respectively), the skin thickness of ^{208}Pb, the L parameter, defined in Eq. (2), and the symmetry pressure P_0. This confirms that the skin is sensitive to the pressure in the neutron-enriched core of ^{208}Pb which pushes excess neutrons towards the low-density edges of the nucleus.

On the other hand, the average density in nuclei is less than saturation density and, therefore, typical nuclear observables (such as, for instance, those used to construct phenomenological forces) actually probe densities somewhat lower than the one of normal saturated matter. Therefore, Table 1 also shows how the slope of the symmetry energy at ρ=0.1 fm^{-3} varies in relation to the neutron skin (third column).

Table 1. Neutron skin (S) of ^{208}Pb with varying power law, γ, in the interaction symmetry energy within the range determined by the ASY-EOS analysis. The third column displays the the slope of the symmetry energy at about 2/3 of saturation density, followed by the L parameter and the symmetry pressure. For further details, see discussion in the text.

γ	S (fm)	$\frac{\partial e_{sym}}{\partial \rho}$ (MeV fm^3)	L (MeV)	P_0 (MeV/fm^3)
0.53	0.14	154	60.1	3.14
0.72	0.18	177	72.6	3.80
0.91	0.21	195	85.2	4.45

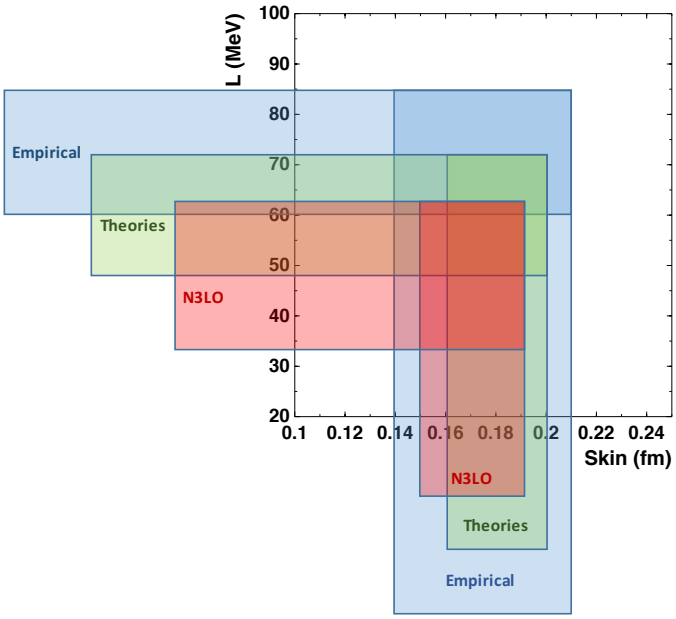

Figure 3. Relation between the L parameter and the neutron skin in ^{208}Pb. Blue shaded area: empirical constraint for L and corresponding constraint for the neutron skin. Green area: Predictions from Table 2. The predictions at N^{3}LO with their truncation error produce the pink region.

The observations collected above can be more easily captured in a visual way, as presented in Figure 3. The area shaded in blue is obtained from the empirical constraint for L and the corresponding constraint for the neutron skin. Including the predictions from Table 2 generate the green area. Finally, the predictions at N^{3}LO with their truncation error produce the pink region. Clearly, the uncertainty in the density derivative is much larger than could be inferred from the blue area, that is, from the correlation based on the empirical information.

In Ref. [4], the authors do mention that the sharp value of $e_{sym}^{pot}(\rho_0)$ is the result of choosing a power law as in Eq. (1) and that using lower values of

Table 2. As in Table 1, but for each of the theoretical approaches under consideration.

Theor. Approach	S (fm)	$\frac{\partial e_{sym}}{\partial \rho}$ (MeV fm^3)	L (MeV)	P_0 (MeV/fm^3)
DBHF	0.16	135	46.8	2.45
N^{3}LO	0.17	148	47.5	2.50
APR	0.18	158	65.0	3.43
N^{2}LO	0.20	176	72.0	3.79

$e^{pot}_{sym}(\rho_0)$ leads to lower values of L, still within acceptable error margins. However, the results from Ref. [16] (which are based on Skyrme phenomenology), are no longer met with the alternative parametrization. The results which have been reviewed here show that adhering to Eq. (1) is not recommendable from the theoretical standpoint.

4 Preliminary Neutron Star Predictions

The EoS provides the link between the structure of compact stars and the physics of neutron-rich nuclei. To investigate the former, EoS predictions must be available at the typical central densities of compact stars, which can exceed several times the density of normal saturated matter.

Chiral EFT is a low-energy theory and thus there are limitations to its domain of validity. First, the chiral symmetry breaking scale, $\Lambda_\chi \approx 1$ GeV, limits the momentum energy regions where pions and nucleons are the appropriate degrees of freedom. Further, the cutoff parameter Λ appearing in the regulator function suppresses high momentum components (which should not impact the prediction of low-energy observables). The degree of suppression depends of course on the strength of the cutoff.

The high densities encountered in the core of neutron stars correspond to Fermi momenta which are outside the reach of chiral EFT and thus methods to extend the predictions must be employed. A reasonable strategy to extrapolate chiral predictions to high densities is based on the consideration that, for a very large number of existing EoS, the pressure as a function of density (or mass density) can be fitted by piecewise polytropes, namely functions of the form $P = \alpha\rho^\Gamma$ [18]. (In our notation, ρ is the baryon density.) With this observation as a guideline, we fit the pressure obtained from the chiral EoS with polytropes and use them to extend the predictions to higher densities.

Figure 4 shows the pressure in neutron matter as a function of density for the chiral EoS at N^{2}LO and N^{3}LO. Note that the predictions at N^{2}LO are necessary to estimate the truncation error, and thus we will include them throughout the paper. The densities between approximately $2\rho_0$ and $3\rho_0$, where ρ_0 has been defined previously, enclose the highest density region at which the calculations have been conducted. Comments are in place concerning the robustness of those predictions. Keeping in mind that our typical cutoff is in the order of 500 MeV, one should consider the possibility of "cutoff artifacts" when the typical momentum for the system under consideration becomes close to that value. Now, at a density of about $2\rho_0$, the Fermi momentum of neutrons in pure neutron matter is approximately 400 MeV. This is the *highest* rather than the typical momentum of the system, which is considerably lower. Thus, we expect the calculations at that density to be sound. For the last calculated density, the highest momentum of the neutrons is about 470 MeV, which is close to the value of our typical cutoff but, again, larger than the average momentum. As a preliminary, exploratory step, we will push the calculation to this limit [7].

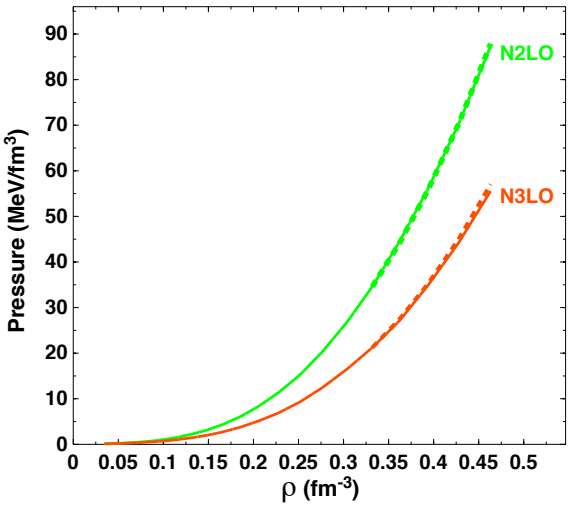

Figure 4. (Color online) Pressure in neutron matter as a function of density at the indicated orders of chiral perturbation theory. The cutoff is equal to 500 MeV. In each case, the dashed curves are polytropes fitted to the high density parts of the predictions.

We fit the high density part of the pressure with a function of polytropic form, $P(\rho) = \alpha\rho^{\Gamma}$, and determine the adiabatic index Γ. In fact, we take the fitting function to be $P(\rho) = P_{2\rho_0}\left(\frac{\rho}{2\rho_0}\right)^{\Gamma}$, with $P_{2\rho_0}$ the theoretical pressure at $2\rho_0$, so that the fit is exact at $2\rho_0$ and well constrained around this density, as seen from Figure 4.

We then use the polytrope to extend the pressure and energy density past the theoretically calculated range. In this way, we exploit the theoretical predictions as long as possible, having gained some confidence from the observation that no cutoff artifacts, which might be signaled by a reduced growth in pressure, are apparent from Figure 4.

We are now in the position to proceed with the solution of the Tolman-Oppenheimer-Volkoff (TOV) [19] star structure equations for central densities up to several times normal density. In this very preliminary step, we will consider stars consisting only of pure neutron matter.

We will focus our attention on the most probable mass of a neutron star, which is approximately 1.4 $M_{\odot}$. For such stars, typical central densities are a few times normal density and, therefore, the predictions rely on the extrapolation to a much lesser extent than for heavier stars, particulary maximum-mass stars.

In Table 3, we report the radii at N^{2}LO and N^{3}LO, respectively, along with cutoff dependence. The results can be stated as:

$$R_{N2LO} = 13.3 \pm 0.3 \qquad R_{N3LO} = 11.6 \pm 0.3\ . \tag{4}$$

Table 3. Radius of a neutron star with M=1.4 $M_\odot$ at the given order and cutoff. In each case, the pressure in neutron matter at ρ_0 is also shown.

Order	Λ (MeV)	R (km)	$P^{NM}_{\rho_0}$ (MeV/fm^3)
N^{3}LO	450	11.34	2.59
	500	11.88	2.46
	600	11.51	2.11
N^{2}LO	450	13.38	3.96
	500	13.53	3.94
	600	12.98	3.34

Estimating the truncation error from the absolute value of the difference between the predictions at N^{2}LO and N^{3}LO (a pessimistic estimate), we quote our current results at N^{3}LO as

$$R_{N3LO} = 11.6 \pm 1.7 \ . \tag{5}$$

Because cutoff uncertainty for the radius appears to be much smaller than the one due to truncation, we will ignore it in later considerations.

The above may help us understand to which degree the pressure in neutron matter around saturation can constrain the radius of a 1.4 $M_\odot$ (pure) neutron star. To that end, we estimate the corresponding uncertainty on the pressure *around saturation* and report the result, at N^{3}LO, as $P^{NM}_{\rho_0} = 2.4 \pm 0.7$ MeV fm^{-3}.

This uncertainty is quite large, and should become smaller in the near future due to both improved experimental constraints and refinements in the theory. One may then conclude that the pressure around saturation is in principle capable of providing a considerable constraint for the radius. In other words, improved knowledge of the density slope of neutron matter at saturation, namely at densities within the reach of terrestrial measurements, is likely to provide stringent boundaries for the radius of the typical-mass neutron star.

We also point out the analysis in Ref. [20], where the overall error was estimated from uncertainty in the many-body forces (due to variations of the cutoff and of the low-energy constants (LECs) c_i appearing in the 3NF and obtained from πN scattering), and from the extrapolation to high densities. The latter was performed using piecewise polytropes which can mimic a large set of existing neutron matter EoS with matching densities as free parameters [18]. The range for the radius of a 1.4 $M_\odot$ pure neutron star was reported to be R=9.3-13.3 km. In a later study [17], a range R=9.7-13.9 km was found for a neutron star with a mass of 1.4 $M_\odot$. (With regard to variations of the πN LECs to estimate the uncertainty in the chiral predictions, we like to point out, in passing, that we disagree with this method in view of most recent and very accurate πN LECs determination [21]. We take the position that order-by-order considerations are the correct way to estimate chiral uncertainties.)

5 Conclusions

Theoretical calculations of the symmetry energy, in particular from modern *ab initio* predictions, are timely and important as they complement on-going and future experimental efforts. Existing predictions for the interaction part of the symmetry energy have been explored in the light of new and more stringent constraints recently obtained for this quantity. We considered a few but fundamentally different approaches to obtain a realistic idea of the spreading in microscopic predictions.

We find that the simplest assumption of a single-term power law does not capture the density dependence of the interaction symmetry energy for the theories which we have considered. The N^{3}LO prediction is generally softer than the constraint.

The focus then moves to the neutron skin thickness of ^{208}Pb. Caution must be excercised with regard to the possibility of constraining the density slope from the knowledge of the skin based only on correlations obtained with families of simple phenomenological interactions, as the latter procedure may underestimate the uncertainties.

We also briefly reviewed our preliminary predictions of neutron star radii, with emphasis on the role of the pressure around normal density in the formation of both the neutron skin and the radius of a typical neutron star. Our ultimate goal is to produce systematic order-by-order predictions of neutron star masses and radii with a β-equilibrated EoS based on chiral EFT.

Acknowledgments

This work was supported by the U.S. Department of Energy, Office of Science, Office of Basic Energy Sciences, under Award Number DE-FG02-03ER41270.

References

[1] Y. Leifels *et al.*, *Phys. Rev. Lett.* **71** (1993) 963.
[2] D. Lambrecht *et al.*, *Z. Phys.* **A 350** (1994) 115.
[3] P. Russotto *et al.*, *Phys. Lett. B* **697** (2011) 471.
[4] P. Russotto *et al.*, *Phys. Rev. C* **94** (2016) 034608.
[5] S. Weinberg, *Phys. Lett. B* **251** (1990) 288.
[6] F. Sammarruca, *Phys. Rev.* C **95** (2017) 044316.
[7] F. Sammarruca, *Modern Physics Letters A*, in press.
[8] F. Sammarruca, L. Coraggio, J. Holt, N. Itaco, R. Machleidt, and L.E. Marcucci, *Phys. Rev. C* **91** (2015) 054311.
[9] D.R. Entem and R. Machleidt, *Phys. Rev. C* **68** (2003) 041001.
[10] J.W. Holt, N. Kaiser, and W. Weise, *Phys. Rev.C* **79** (2009) 054331; *Phys. Rev. C* **81** (2010) 024002.
[11] H. Müther, F. Sammarruca, and Z. Ma, *Int. J. Mod. Phys. E* **26** (2017) 1730001, and references therein.

[12] A. Akmal and V.R. Pandharipande, *Phys. Rev. C* **56** (1997) 2261.
[13] A. Akmal, V.R. Pandharipande, and D.G. Ravenhall, *Phys. Rev. C* **58** (1998) 1804.
[14] R.B. Wiringa, V.G.J. Stoks, and R. Schiavilla *Phys. Rev. C* **51** (1995) 38.
[15] B.S. Pudliner, V.R. Pandharipande, J. Carlson, and R.B. Wiringa, *Phys. Rev. Lett.* **74** (1995) 4396.
[16] B.A. Brown, *Phys. Rev. Lett.* **111** (2013) 232502.
[17] K. Hebeler and A. Schwenk, *Eur. Phys. J. A* **50** (2014) 11.
[18] J.S. Read *et al.*, *Phys. Rev. D* **79** (2009) 124032.
[19] J.R. Oppenheimer and G.M. Volkoff, *Phys. Rev. C* **55** (1939) 374.
[20] K. Hebeler, J.M. Lattimer, C.J. Pethick, A. Schwenk, *Phys. Rev. Lett.* **105** (2010) 161102.
[21] M. Hoferichter *et al.*, *Phys. Rev. Lett.* **115** (2015) 192301; *Phys. Rep.* **625** (2016) 1.